Journal of Pharmaceutical Analysis 14 (2024) 101105

Contents lists available at ScienceDirect

Journal of Pharmaceutical Analysis

journal homepage: www.elsevier.com/locate/jpa

Original article

Integrating transcriptomics, metabolomics, and network pharmacology to investigate multi-target effects of sporoderm-broken spores of *Ganoderma lucidum* on improving HFD-induced diabetic nephropathy rats

Lidan Hu [a, 1], Lili Yu [b, c, 1], Zhongkai Cao [a, 1], Yue Wang [d], Caifeng Zhu [e], Yayu Li [e], Jiazhen Yin [e], Zhichao Ma [a], Xuelin He [f], Ying Zhang [g], Wunan Huang [a], Yuelin Guan [a], Yue Chen [h, ***], Xue Li [c, **], Xiangjun Chen [g, *]

[a] *Department of Nephrology, The Children's Hospital, Zhejiang University School of Medicine, National Clinical Research Center for Child Health, Hangzhou, 310003, China*
[b] *Centre for Global Health, Usher Institute, The University of Edinburgh, 5-7 Little France Road, Edinburgh, EH16 4UX, UK*
[c] *Department of Big Data in Health Science School of Public Health, Zhejiang University School of Medicine, Hangzhou, 310058, China*
[d] *Hubei Normal University. No. 11, Cihu Road, Huangshi, Hubei, 435002, China*
[e] *Department of Nephrology, Hangzhou TCM Hospital, Hangzhou, 310007, China*
[f] *Kidney Disease Center, The First Affiliated Hospital, Zhejiang University School of Medicine, Hangzhou, 310003, China*
[g] *Institute of Translational Medicine, Zhejiang University School of Medicine, 268 Kaixuan Road, Hangzhou, 310020, China*
[h] *Department of Urology, The Second Hospital of Tianjin Medical University, Tianjin Institute of Urology, Tianjin, 300211, China*

ARTICLE INFO

Article history:
Received 11 March 2024
Received in revised form
24 August 2024
Accepted 13 September 2024
Available online 19 September 2024

Keywords:
Diabetic nephropathy
Metabolome
Network pharmacology
Sporoderm-broken spores of *Ganoderma lucidum*
Transcriptome

ABSTRACT

Diabetes mellitus (DM) is a major metabolic disease endangering global health, with diabetic nephropathy (DN) as a primary complication lacking curative therapy. Sporoderm-broken spores of *Ganoderma lucidum* (GLP), an herbal medicine, has been used for the treatment of metabolic disorders. In this study, DN was induced in Sprague-Dawley rats using streptozotocin (STZ) and a high-fat diet (HFD), and the protective mechanisms of GLP were investigated through transcriptomic, metabolomic, and network pharmacology (NP) analyses. Our results demonstrated that GLP intervention ameliorated renal damage and inflammation levels in DN rats. Integrative metabolomic and transcriptomic analysis revealed that GLP treatment modulated glucose and cellular energy metabolisms by regulating relevant genes. GLP significantly suppressed the inflammations by impacting glucose and energy metabolism-related gene expression (*Igfbp1* and *Angptl4*) and enhanced metabolic biomarkers of 4-Aminocatechol. In addition, NP analysis further indicated that GLP may efficiently alleviate DN via immune-related pathways. In conclusion, this study provides supportive evidence of the anti-inflammatory effects of GLP supplements, highlighting their potential for promising clinical applications in treating DN.

1. Introduction

Diabetes mellitus (DM) is one of the major diseases endangering global health, which is expected to affect 439 million people worldwide by 2030 [1]. Metabolic alterations brought on by DM can lead to major microvascular conditions, including retinopathy, neuropathy, and diabetic nephropathy (DN) [2,3]. Further, it is reported that pathological characteristics of DN include extracellular matrix accumulation in renal interstitial tissue, glomerular mesangial expansion, glomerular sclerosis and hypertrophy [4]. Numerous research has indicated that the initiation and development of DN are induced by multiple factors, including diet factors, genetic alterations, early-stage hyperperfusion and hyperfiltration of aberrant renal hemodynamics, and metabolic disorders induced by hyperglycemia [5]. Currently, few effective and safe medicines are available to treat DN. Therefore, there is a need to search safe and effective drugs to prevent DN progression.

* Corresponding author.
** Corresponding author.
*** Corresponding author.
E-mail addresses: chenyue831106@126.com (Y. Chen), xueli157@zju.edu.cn (X. Li), chenxiangjun@zju.edu.cn (X. Chen).
[1] These authors contributed equally to this work.

https://doi.org/10.1016/j.jpha.2024.101105

The traditional Chinese medicine (TCM) utilized for thousands of years in clinic is thought to be multi-targeting. A growing body of studies have shown that compounds derived from TCM might lower the likelihood of bronchitis, allergies, immunological disorders, and cancers in a variety of ways [6,7]. For generations, a well-known herbal medicinal mushroom, *Ganoderma lucidum* (*G. lucidum*), has been utilized in Asian therapeutic settings for over 2000 years to improve the immune system, extend longevity, and maintain overall health [8], and has long been considered a magical or spiritually potent herb in China [8]. Sporoderm-broken spores of *Ganoderma lucidum* (GLP) contain a wider range of bioactive compounds, including triterpenes, polysaccharides, proteins, fatty acids, and nucleosides. They have been widely recognized for original pharmacological values, which include anti-inflammatory effects, anticancer, anti-aging, antioxidant, and hypoglycemic properties [9,10]. And GLP also contributes to preventing the rapid metabolism of other active components, improving loading rate and encapsulation efficiency of ingredients, and ultimately enhancing the bioactivity and pharmacological effects as nano-systems [11,12]. The traditional uses of GLP are remarkably extensive, encompassing a wide range of health conditions and disease states. These include, but are not limited to metabolic disorders such as diabetes and metabolic syndrome; cardiovascular conditions like hypertension and hyperlipidemia; chronic diseases affecting the liver, kidneys, and respiratory system; neurological disorders including Alzheimer's and Parkinson's diseases; various types of cancers; autoimmune conditions such as rheumatoid arthritis and lupus [13–15].

DN is a complex disorder involving various pathological processes, including inflammation, oxidative stress, metabolic dysregulation, and fibrosis. The multifaceted pharmacological profile of GLP positions it as a more promising candidate for addressing the complex pathophysiology of DN compared to single-target interventions. Previous studies have shown that *G. lucidum* polysaccharides could reduce inflammatory markers such as interleukin (*IL*)-*6*, *IL-1*β, and tumor necrosis factor-alpha (*TNF-*α), which play significant roles in DN pathogenesis [16,17]. Also, *G. lucidum* polysaccharides reduce proteinuria, serum creatinine levels, and renal hypertrophy, thus indicating protective effects on kidney function in DN models [18]. Additionally, GLP improves glucose metabolism and insulin sensitivity by modulating key metabolic pathways [16,19]. Therefore, GLP may be a potentially safe and effective therapy for DN. Nevertheless, above-mentioned existing evidence of GLP on DN typically concentrated on a single clinical feature [20,21]. The multi-therapeutic effects of GLP on DN have not been elucidated.

More recently, novel advances in genomics, transcriptomics, and metabolomics have revolutionized the search for therapeutic targets [22]. Additionally, network pharmacology (NP) method integrates conventional pharmacology, biology of systems and biochemistry, drug interactions and activities with multiple key targets that could be systematically elucidated. Herein, a multi-omics approach, including transcriptomics, metabolomics, and NP analysis in this study, allows for a more comprehensive understanding of the molecular mechanisms underlying GLP's effects. This multi-omics approach can provide insights into the complex interactions between GLP and the biological systems involved in DN, potentially uncovering novel therapeutic targets and pathways.

2. Materials and methods

2.1. Materials

GLP was manufactured using the following methods: harvesting, spore collection, purification, drying, sporoderm-breaking, and extraction. In short, the fluidized-bed air-flow mill was firstly used to break the complete *G. lucidum spore polysaccharide* (raw material), and removed the sporoderm by filtration, purification, concentration, and drying to produce the so-called GLP. It was supplied by Zhejiang Jibaichuan Pharmaceutical Co., Ltd., which was acquired from the cultivation in Hangzhou, Zhejiang, China (batch No. 20230105). This product was approved under drug production license No. 20190017. The product of GLP is brown powder with slight odor and light or slightly bitter taste. Its characteristic components such as polysaccharide (%) shall not be less than 0.8, and triolein (%) shall not be less than 3.0. Its physical and chemical indicators such as moisture (%) shall not exceed 9.0, total ash (%) shall not exceed 3.0, impurities shall not be detected with foreign matter such as mycelium and starch, and shall be tested under a microscope; the difference in filling volume shall comply with the regulations: 1 g/bag (0.94–1.06 g), 2 g/bag (1.90–2.10 g), 5 g/bag (4.75–5.25 g), 50 g/can (50–52.5 g), 100 g (100–103 g); lead shall not exceed 2 parts per million, cadmium shall not exceed 5 parts per million, arsenic shall not exceed 1 part per million, mercury shall not exceed 1 part per million, copper shall not exceed 20 parts per million, chromium shall not exceed 2 parts per million, and nickel shall not exceed 1 part per million. The wall breaking rate shall not be less than 95%, the peroxide value shall not exceed 0.20. Its microbial indicators are total aerobic bacteria (cfu/g) less than or equal to 40,000, mold and yeast (cfu/g) less than or equal to 50, *Escherichia coli* (MPN/g) less than or equal to 0.92, and Salmonella less than or equal to 0/25 g. The detection method shall be in accordance with the "Chinese Pharmacopoeia" and "Zhejiang Province Traditional Chinese Medicine Processing Specifications".

2.2. Animals and treatments

From the Shanghai laboratory animal centre, nine adult male Sprague-Dawley rats (eight weeks, weight: 180–200 g) were acquired, and they were fed in a free of bacteria environment. All rats were kept in well-regulated environments (12 h of light/dark, 22 ± 1 °C), with unlimited availability of distilled water and food. All experimental operations were fully adhered to the Institutional Animal Care and Use Committee of Zhejiang University, as well as Provision and General Recommendation of the Chinese Laboratory Association. After adaptive feeding for one week, rats were randomly assigned to three groups ($n = 5$, respectively): the Control group, high-fat diet (HFD)-fed group (DN) and GLP-treated HFD-fed group (DN + GLP). Rats were given a high-sugar and HFD for four weeks in both DN and DN + GLP (60% kcal fat, 20% kcal protein, and 20% kcal carbohydrate, #D12492; Research Diets, New Brunswick, NJ, USA). The ingredient of HFD contains 4057 kcal, including 800 kcal Casein-80 Mesh, 12 kcal L-Cystine, 500 kcal L-Cystine, 275.2 kcal Sucrose, 275.2 kcal Soybean, 2205 kcal Oil Lard*, 40 kcal Vitamin Mix. The detailed manufacturing process about the HFD is as follows. The first step is the generation of a batch ticket which we call a Production Checklist (PCL). The PCL is prepared electronically and is scaled for the specified batch size. Each batch of diet is prepared by a trained diet technician who works under the direct supervision of the Production Manager. The macros are also enabled to verify that the Research Diets, Inc. (RDI) Lot Number entered for each ingredient. Upon completion of blending, the Production Manager will inspect the batch and notify the Pelleting Manager (PM) that the batch is ready for pelleting. The PM also ensures that additional information such as the pellet mill used to produce the pellets, the type of die used, and various other parameters are documented on the PCL for this batch. Upon completion of the pelleting stage, the diet is placed into a temperature- and humidity-controlled room so that moisture can be removed from the product after two days drying. If determined to be dry, then the diet can be removed from the drying room for

sampling and packaging. A regular diet (#P1300F, Hangzhou Cellojin Biotechnology Co., Ltd., Hangzhou, China) was provided to the Control group. Then, rats in both DN group and DN + GLP group received an intraperitoneal injection of streptozotocin (STZ) (40 mg/kg, # CSN11987, CSNpharm, Hangzhou, China) after fasting for 16 h in the fifth week. In order to generate a diabetic model, STZ was dissolved in 0.1 M sodium citrate buffer (#T108601 Yonghua Chemical Technology (Jiangsu) Co., Ltd., Changshu, Jiangsu, China, pH 4.4). Equal doses of sodium citrate buffer were given to rats in the Control group. Fasting blood glucose levels in rats were detected 72 h following the injection, by piercing the ventral tail vein, samples were taken using a one-touch glucose analyser. Rats with blood glucose levels higher than 16.7 mmol/L were confirmed as DN rats and were selected for further study. The DN + GLP group was treated with GLP of 200 mg/kg every two days, while normal saline was given to the DN and Control groups. The dose of 200 mg/kg can be regarded as low dose to explore the potential effect of GLP treatment, meanwhile, avoiding side toxicity along with long periods of GLP treatment based on supporting evidence [23–25].

For each week after inducing DN model, measurements of body weight and blood glucose were taken in this study. Rats were fasted for 12 h before the blood and urine collection following the 17-week intervention. After centrifuging 200 μL of serum for 20 min at 4 °C, the samples were stored at −80 °C. Following an assessment of the body weight, rats were euthanized, and kidney tissues were obtained and preserved at −80 °C for further biochemical tests and pathological assessment, and the ratio of kidney/body weight was calculated.

2.3. Histological assessment

The kidney tissue of rats was fixed, sliced, and sealed, and then stained with hematoxylin-eosin (H&E, #G1120, Solarbio, Beijing, China) and Masson's trichrome (#G1346, Solarbio, Beijing, China). With routine treatment, H&E and Masson's trichrome staining were applied to adipose tissue of epididymis, respectively. Inverted Fluorescence Microscope (LSM900, Zeiss, Netherlands) was utilized immediately to observe the histopathological changes. In regard as transmission electron microscopy (TEM), small pieces (1 mm × 1 mm × 1 mm) of kidney cortex were fixed in 2.5% glutaraldehyde in 0.1 M cacodylate buffer (pH 7.4) for 2 h at 4 °C. Samples were post-fixed in 1% osmium tetroxide for 1 h, then dehydrated through a graded ethanol series. Tissues were embedded in Epon 812 resin. Ultrathin sections (60–80 nm) were cut using an ultramicrotome and collected on copper grids. Sections were stained with uranyl acetate and lead citrate. Samples were examined using a Thermo FEI Tecnai G2 spirit transmission electron microscope. Small pieces (1 mm × 1 mm × 1 mm) of kidney cortex were fixed in 2.5% glutaraldehyde in 0.1 M cacodylate buffer (pH 7.4) for 2 h at 4 °C in scanning electron microscopy (SEM) analysis. Samples were washed three times with 0.1 M phosphate buffer, then post-fixed with 1% osmium tetroxide for 2 h. Tissues were dehydrated through a graded ethanol series (30%, 50%, 70%, 90%, and 100%). Samples were critical point dried, mounted on aluminum stubs, and sputter-coated with gold-palladium. Specimens were examined using a Thermo FEI Nova Nano 450 scanning electron microscope. Glomerular diameter was measured digitally for standardizing the degree of glomerular damage, taking the average of glomerular width and height from individual glomeruli. 10 random complete glomeruli with both hilum and urinary pole from 30 randomly selected fields of each animal were used as the glomerular damage index for each animal. Glomerular sclerosis percentages were assessed by recording the number of sclerotic glomeruli in a total of 10 randomly selected fields of glomeruli. The percentage of glomerular sclerosis was calculated as elation sclerotic glomeruli/total glomeruli number. Tubular injury scores were scored using a semiquantitative grading system, evaluating on a scale of 0–4 as follows: 0, no tubulointerstitial injury; 1, < 25% injury; 2, 25%–50% injury; 3, 51%–75% injury; and 4, > 75% injury. The higher the score is, the more severe the renal tubular injury is. 10 randomly selected fields in each mouse were examined for the presence of tubules sclerotic lesions.

2.4. RNA extraction and nephritic transcriptome analysis

The TIANGEN RNAprep Pure Cell Kit (# DP431, Tiangen Biochemical Technology (Beijing) Co., Ltd., Beijing, China) and TRIzol reagent (# 9109, Takara, Beijing, China) were used to isolate total RNA from three separate kidney cells and kidney tissue samples from each group, respectively. PrimeScript™ RT Master Mix (# RR036A, Takara, Beijing, China) was applied to perform reverse transcription and library construction using 1 μg of total RNA in accordance with the instructions of manufacturer. Utilizing Illumina TruSeq™ RNA sample preparation kit to construct sequencing libraries and then performed on Illumina HiSeq X Ten platform in a 2 × 150 bp paired-end configuration. After removing the connector sequence and low quality reads, the original reads were converted into clean reads alignment with the mouse reference genome (mRatBN7.2) by bowtie2, to obtain mapping data. The fragments per kilobase million (FPKM) algorithm was used to assess the ability of RNA transcripts to discriminate Control, DN and DN + GLP samples by incorporating principal component analysis (PCA). Taking raw counts as the original expression amount of the gene, "DESeq2" R package was implemented to screen differentially expressed genes (DEGs) with a filter threshold of fold change (FC) ≥ 1 and Benjamini and Hochberg (BH)-corrected false discovery rate (P_{FDR}) < 0.05. To annotate DEGs, Gene Ontology (GO) and Kyoto Encyclopedia of Genes and Genomes (KEGG) databases were applied to elucidate the potential enrichment pathways.

2.5. Untargeted nephritic metabolome analysis

Kidney samples that had been collected were extracted using a 20% methanol solution and processed according to previously published techniques. Equal quantities of each extracted supernatant were combined to create a pooled quality control (QC) sample, which was then injected on a regular basis (every three samples). By applying an ultra-high pressure liquid chromatography (UHPLC) system in conjunction with a triple quadrupole time of flight (TOF) analyzer (Waters, Milford, MA, USA), all extracted metabolites were examined. An hydrophilic interaction liquid chromatography (HILIC) TSK gel Amide-80 column (250 mm × 2.0 mm, i.d., 5 μm) with a 2.0 mm × 1 cm i.d. guard column of the same material provided by Tosoh Bioscience (Tokyo, Japan) was used for analytical separation of metabolites. The flow rate was 0.15 mL/min and elution gradient was performed using solvent A (acetonitrile) and solvent B (ammonium acetate 3 mM at pH5.5, adjusted with acetic acid) as follows: 0–3 min, isocratic gradient at 5% B; 3–27 min, linear gradient from 5% to 70 % B; 27–30 min, isocratic gradient at 70% B; 30–32 min back to the initial conditions at 5% B; and from 32 to 40 min, at 5% B. The full scan mode of the positive electrospray ionisation was applied to operate mass spectrometer (MS). For variations in the lockmass, the spectral peaks were automatically corrected.

MSConvert function of ProteoWizard was used to convert MS raw data files into the mzML format. Log-transformed processed raw liquid chromatography-tandem mass spectrometry (LC-MS) data were identified using the Metlin database. The scaled and normalised data were then imported into R software ("Ropls" R package) for multivariate analysis, incorporating principal

component analysis (PCA) and orthogonal partial least squares discriminant analysis (OPLS-DA). To confirm differential metabolites, the following criterions were used: FC (FC > 1 or < 0.5), variable importance (VIP) (VIP > 1) value, and *P* value ($P < 0.05$). MetaboAnalyst 5.0 (https://www.metaboanalyst.ca/) was utilized to perform KEGG metabolic pathway enrichment analysis based on the differential metabolites that were found.

2.6. Transcriptome and metabolomics integration

The associations between identified differentially expressed gene signatures and the normalised differential metabolites were calculated using Spearman's correlation coefficients. A scaled heatmap was created for the correlation matrix using the default clustering method. Nominal *P* values ($P < 0.05$) were reported for signature testing.

2.7. Network pharmacological analysis

The OMIM (https://www.omim.org/), GeneCards (https://www.genecards.org/), and PharmGKB (https://www.pharmgkb.org/) databases were searched for target information pertaining to the active drug components of GLP. The UniProtKB (https://www.uniprot.org/) database was used to convert the target proteins and gene names into standard target names. To obtain the DN-relevant targets, "Diabetic Nephropathy" was searched as keywords in DrugBank (https://www.drugbank.com/), DisGeNET (https://www.disgenet.org/), therapeutic target database (TTD) (https://db.idrblab.net/ttd/), and GeneCards (https://www.genecards.org/). Similarly, gene symbol transformation of disease targets was carried out using the Uniprot database (https://www.uniprot.org/). Duplicates of the four databases were removed to obtain disease target signals. Subsequently, the common targets of DN and GLP, which were thought to be prospective targets in this study, were obtained via the website (http://bioinformatics.psb.ugent.be/webtools/Venn/).

The PPI network was constructed using these plausible targets in the STRING database (https://string-db.org/), with a medium confidence parameter of 0.400. Through the Closeness and Degree topological analysis methods, the top 10 proteins were identified by analysing the topological features of the constructed network model applying the CytoHubba function in Cytoscape software. To examine the KEGG enrichment pathways of the targets of GLP acting on DN, the string database and ChiPlot tool were utilized. Moreover, to visualise and create the target-pathway network diagram, the top 20 pathways and identified key targets were uploaded into Cytoscape software.

2.8. Quantitative polymerase chain reaction (qPCR) and biochemical assays

The renal tissue samples and blood samples of animal modelling were collected to estimate the senescence-associated expression of *p16, p21, p27* and *p53*, and inflammation levels (including *IL-1β, IL-6, TNF-α, IL-10, m*atrix metallopeptidase 3 (*MMP3*), *m*onocyte chemoattractant protein-1 (*MCP-1*), C-reactive protein (*CRP*), C-X3-C motif chemokine receptor 1 (*CX3CR1*), C-X-C motif chemokine ligand (*CXCL*)*6* and *LIT*) according to qPCR as described previously, respectively. From the differential expressed genes and enrichment pathways, we selected eight genes (*Igfbp1*, *Angptl4, Map3k13, Slc31a2, Abcb1b, Slc6a9, Slc5a1* and *Erbb3*) involving in glucose metabolism-related and energy metabolism-related to validate our findings. Reverse transcription was carried out in a thermocycler, and qPCR (Applied BiosystemsTM, QuantStudio 5) was carried out in triplicates utilizing complementary DNA (cDNA) templates and a SYBR green master mix (# 11201ES08, Yeason, Shanghai, China) with particular primers. Each sample was measured for three times. Using the $2^{-\triangle\triangle Ct}$ techniques, the relative expression level of the corresponding messenger RNAs (mRNAs) was measured. Table S1 displays the primer sequences used in this study. Utilizing Primer-BLAST from the NCBI webtool (https://www.ncbi.nlm.nih.gov/tools/primer-blast/), we designed certain primer pairs. Serum creatinine was measured using a commercial kit (BIOSINO, Beijing, China).

2.9. Western blot analysis

The nephridial tissue was homogenized using the phenylmethylsulfonyl fluoride (PMSF)- and protease-inhibiting ultrasonic cell disruptor in RIPA lysis buffer (# BL504A, Biosharp, Hangzhou, China) on ice. The proteins were transferred to nitrocellulose membranes after being separated using 12% sodium dodecylsulphate polyacrylamide gel electrophoresis (SDS-PAGE) (# NO. C631100, Sangon Biotech, Shanghai, China). After 1 h of room temperature incubation with blocking buffer (5% BSA) (# NO. B600036, Sangon Biotech, Shanghai, China), the cells were then incubated with primary antibodies for an additional overnight at 4 °C. The horseradish peroxidase-conjugated secondary antibody was incubated for 2 h at the standard room temperature. Finally, using the ECL detection kit (# BL520A, Biosharp, Hangzhou, China), the immunoblots were established, and the band intensity was measured by ImageJ software.

2.10. Statistical analysis

The results represented at least three independent experiments or five rats at least in each group. Prism 9.5 (GraphPad, La Jolla, CA, USA) software was used for statistical analysis on the experimental measurement data, which were presented as mean ± standard error of the mean (SEM). The unpaired two-tailed Student's *t*-test was performed to examine two group comparisons. One-way analysis of variance (ANOVA) with Tukey's post-hoc test was applied for multiple comparisons. $P < 0.05$ was regarded as statistically significant.

3. Results

3.1. Effects of GLP supplementation on preventing DN-induced nephritic function in rats

Schematic workflow of the animal experiments schedules was presented in Fig. 1A. The DN group showed obvious weight loss based on 17-week of induced modelling DN, with rats exhibiting a decreasing trend in body weight in DN (419.00 ± 19.73 g) compared to Control (554.67 ± 29.77 g) (Fig. 1B), as previous studies reported [26,27]. Compared with the Control group (5.74 ± 0.17 mmol/L), the fast blood glucose level (20.82 ± 0.64 mmol/L) was significantly higher in the DN group, whereas no significant change was observed in DN + GLP group (20.65 ± 0.23 mmol/L) (Fig. 1C). Kidney/body weight showed a significant increase in DN group when compared to Control, however, no significant changes were observed in DN + GLP compared with DN group (Fig. 1D). The urine creatinine was observed to evaluate the renal function in the induced DN model. Consistent with the previous report, the activity levels of urine creatinine were higher in the DN group (83.00 ± 56.63 μmol/L) than the Control group (139.67 ± 41.19 μmol/L), while they were significantly much lower in the DN + GLP group (37.67 ± 17.79 μmol/L) in comparison to DN group (Fig. 1E). Fig. S1A consistently showed higher urine proteins level in DN group compared to Control group. DN has been reported to induce cellular

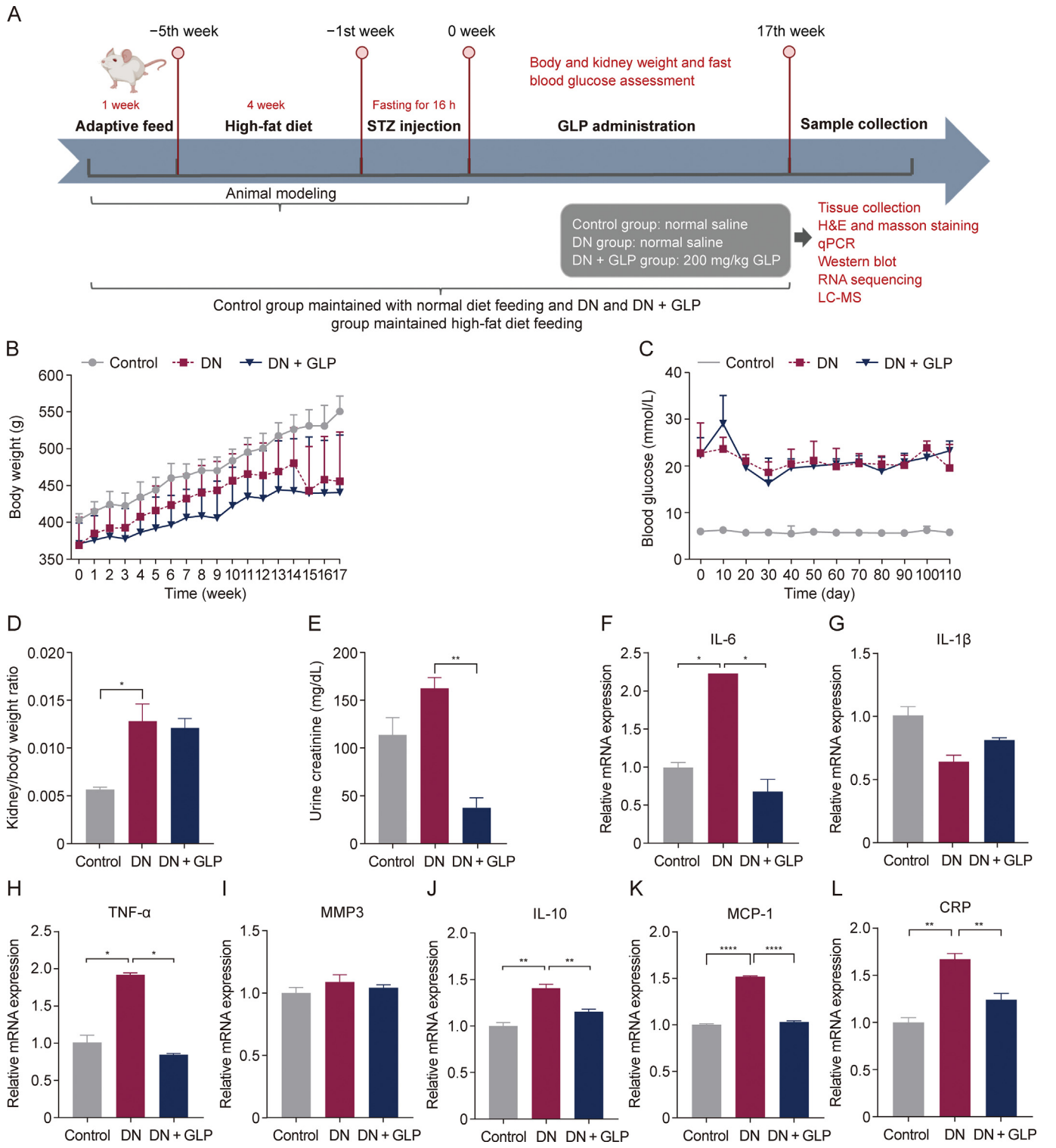

Fig. 1. Experimental design workflow and amelioration of sporoderm-broken spores of *Ganoderma lucidum* (GLP) in this study. (A) Schematic of the experimental design. (B) Body weight. (C) Fasting blood glucose. (D) Kidney/body weight ratio. (E) Urine creatinine. (F–L) Inflammatory cytokines including interleukin (*IL*)-6 (F), *IL-1β* (G), tumor necrosis factor-alpha (*TNF-α*) (H), matrix metallopeptidase 3 (*MMP3*) (I), *IL-10* (J), monocyte chemoattractant protein-1 (*MCP-1*) (*K*) and C-reactive protein (*CRP*) (*L*). Values are presented as mean ± standard error of the mean (SEM) ($n = 5$ in each group). Student's *t*-test was used for comparing Control vs. diabetic nephropathy (DN) and DN vs. GLP-treated high-fat diet (HFD)-fed group (DN + GLP). $^{*}P < 0.05$, $^{**}P < 0.01$, $^{****}P < 0.0001$. mRNA: messenger RNA; STZ: streptozotocin; H&E: hematoxylin-eosin; qPCR: quantitative polymerase chain reaction; LC-MS: liquid chromatography-tandem mass spectrometry.

senescence [28]. Thus, we also examined the changes of senescence-associated expression of *p16, p21, p27* and *p53* among the three groups. As expected, DN group showed a significant increase of *p16, p21, p27* expression level compared to Control, and GLP treatment markedly and significantly attenuated the expression of these senescence-associated markers (Figs. S1B–E). Blood inflammatory cytokines (*IL-1β, IL-6, TNF-α, IL-10, MMP3, MCP-1* and *CRP*) were measured. *IL-6, TNF-α, IL-10, MCP-1* and *CRP* levels were

significantly higher in DN group when compared to Control group. And *IL-6, TNF-α, IL-10, MCP-1* and *CRP* in the DN + GLP groups significantly lowered following GLP treatment as compared with DN group under the same dietary intervention (Figs. 1F–L). These findings suggested the better anti-inflammatory activity of GLP treatment.

Furthermore, we found that GLP ameliorated DN-induced renal damage (Figs. 2A and B). Non-diabetic rats displayed normal tissue with well-organized cell layers, whereas inflammatory infiltration and neovascularization were discovered in DN group (Fig. 2A). According to Fig. 2B, the DN rats showed the increased Masson trichrome-positive areas within the injured glomerulus and tubulointerstitial compartment compared to non-diabetic rats. Notably, GLP treatment apparently improved those morphologic lesions with lower fibrosis and inflammatory infiltration. Glomerular diameter, glomerular sclerosis ratio, and tubular injury scores were measured to observe glomerular and renal injury (Figs. 2C–E). Notably, treatment with GLP markedly improved renal injury compared with DN rats in regards of tubular injury scores (Fig. 2E). Likewise, compared with Control group, TEM analysis showed

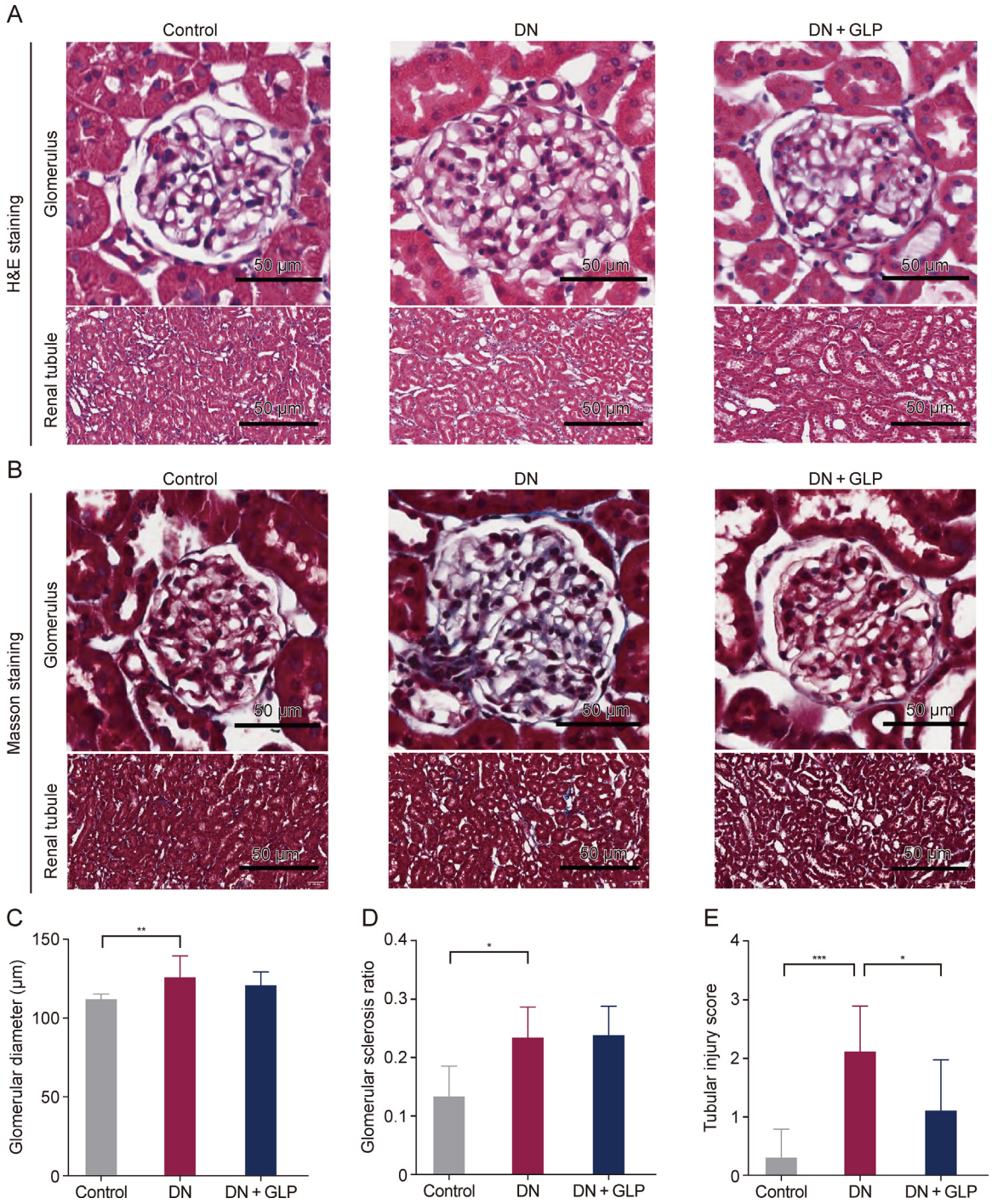

Fig. 2. Amelioration of sporoderm-broken spores of *Ganoderma lucidum* (GLP) on high-fat diet (HFD)-induced diabetic nephropathy (DN) rats. (A, B) Representative histology of glomerulus and renal tubule were assessed by hematoxylin-eosin (H&E) staining (A) and Masson staining (B), respectively. (C–E) Glomerular diameter (C), glomerular sclerosis ratio (D), and tubular injury scores (E) were measured to observe glomerular hypertrophy and renal injury. $^{*}P < 0.05$, $^{**}P < 0.01$, $^{***}P < 0.001$. DN + GLP: GLP-treated HFD-fed group.

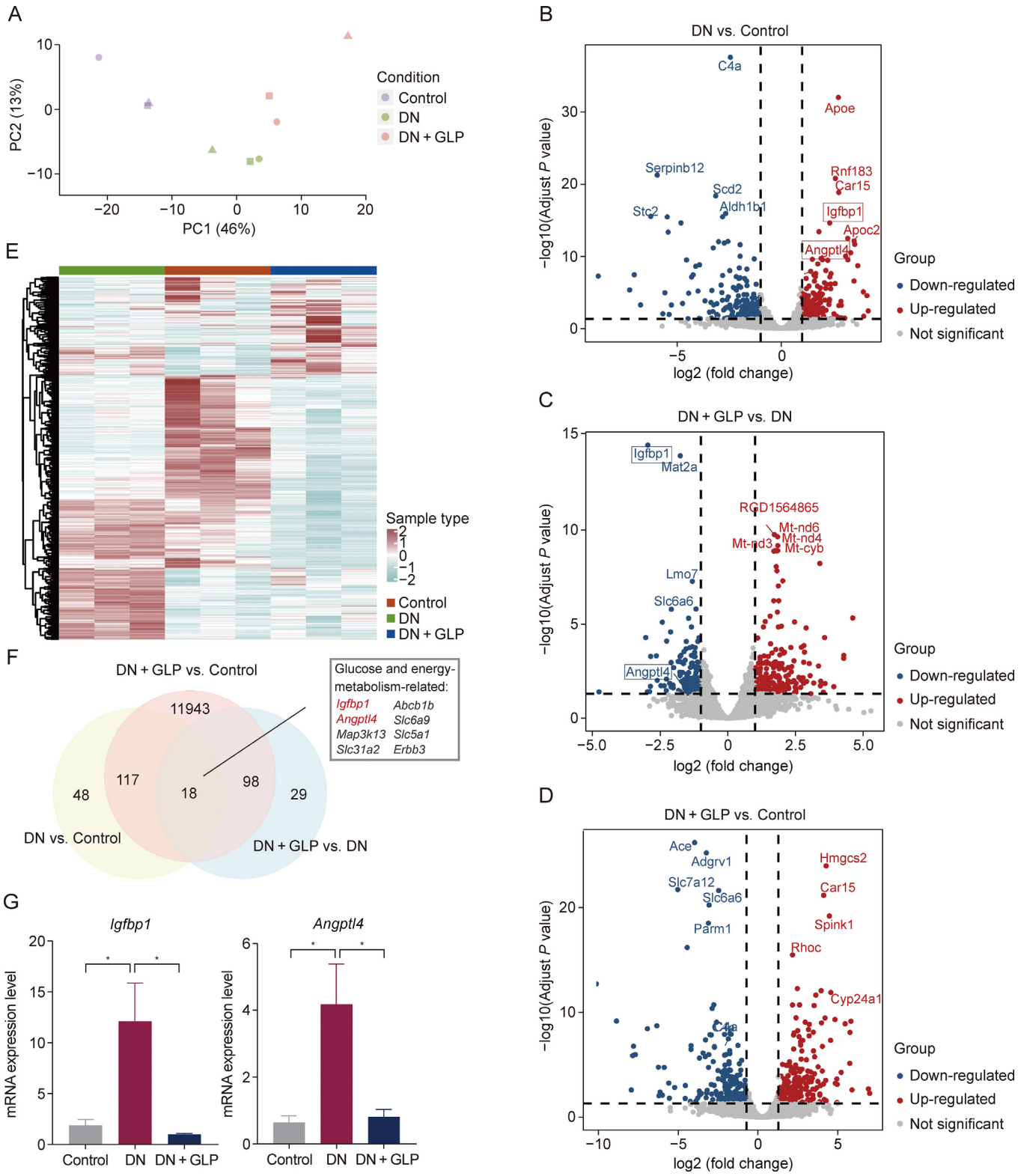

Fig. 3. Effects of sporoderm-broken spores of *Ganoderma lucidum* (GLP) treatment on kidney transcriptome. (A) Principal component analysis (PCA) plot. (B–D) Volcano plot of significant differentially expressed genes (DEGs) of diabetic nephropathy (DN) vs. Control (B), GLP-treated HFD-fed group (DN + GLP) vs. DN (C), and DN + GLP vs. Control (D). Red dots, upregulated; blue dots, downregulated. (E) The heatmap analysis of DEGs in Control, DN and DN + GLP groups. Red, upregulated differential genes; green, downregulated differential genes. (F) Venn diagram of the 18 expression signals consistently upregulated in DN vs. Control group, downregulated in DN + GLP vs. DN group, and no changes in DN + GLP vs. Control group. (G) Quantitative polymerase chain reaction (qPCR) results of glucose and energy-related top-ranking genes of *Igfbp1* and *Angptl4*. $^{*}P < 0.05$. PC: principal component.

severe podocyte foot processes fusion or effacement in DN group, and results of SEM indicated that some podocyte foot processes exhibited fusion and disordered arrangement relative to DN group. After treatment with GLP, the foot process effacement ameliorated, suggesting the protective effects of GLP against podocyte injury (Fig. S2A). Further western bolt analysis visualized that DN group showed a statistically significant increase in the Bax/Bcl-2 ratio compared to Control group, and DN + GLP group lowered the Bax/Bcl-2 ratio compared with DN group, indicating the amelioration of GLP treatment via controlling cellular apoptosis (Figs. S2B and C).

3.2. Effects of GLP supplementation on nephritic transcriptome

Kidney tissue samples were extracted for RNA sequencing (RNAseq) analysis from Control, DN, and DN + GLP groups. DN and DN + GLP intervention groups were distinguished from Control group according to PCA analysis, and principal component 1 (PC1) filtering separated DN + GLP from DN and Control group, which accounted for 46% (Fig. 3A). 444 DEGs were found in DN group compared to Control group from differential expression analysis, among which 189 DEGs were downregulated and 255 DEGs were

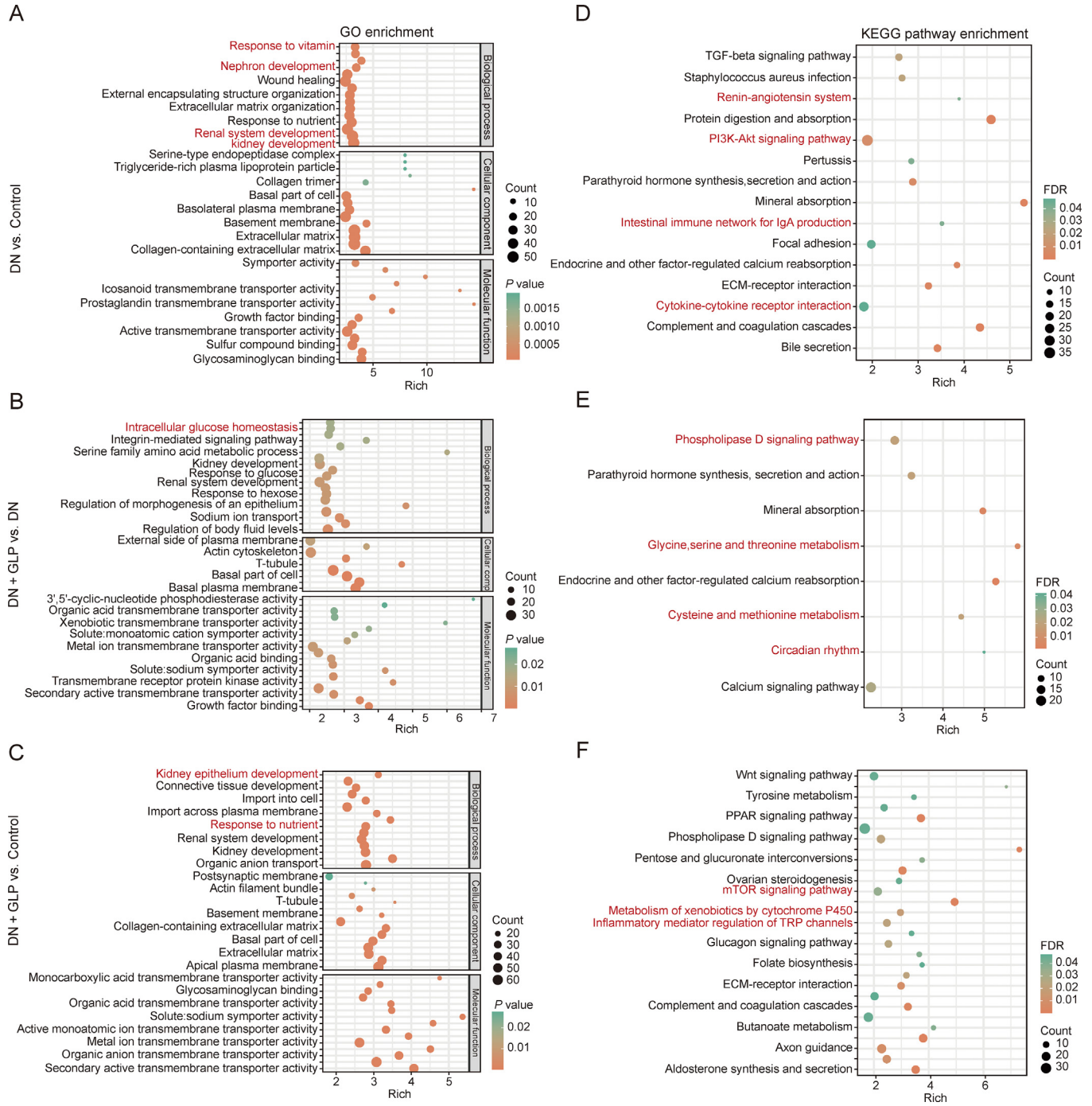

Fig. 4. Gene Ontology (GO) enrichment analysis and Kyoto Encyclopedia of Genes and Genomes (KEGG) enrichment analysis of differentially expressed genes (DEGs). (A–C) Bubble diagram of GO enrichment analysis in diabetic nephropathy (DN) vs. Control (A), GLP-treated high-fat diet (HFD)-fed group (DN + GLP) vs. DN (B), and DN + GLP vs. Control (C). (D–E) Bubble diagram of KEGG enrichment analysis in DN vs. Control (D), DN + GLP vs. DN (E), and DN + GLP vs. Control (F). Size of dots represents genes number in each GO term and KEGG term.

upregulated, respectively (Fig. 3B and Table S2). In comparison to DN, 348 DEGs were identified in DN + GLP (Fig. 3C and Table S3), in addition, GLP treatment induced 507 DEGs compared to Control (Fig. 3D and Table S4). Key DEGs were presented using a heatmap (Fig. 3E). Notably, a total of 18 DEGs were upregulated in DN compared to Control group, whereas the expression levels were consistently downregulated in DN + GLP compared to DN group. Among them, eight genes (*Igfbp1*, *Angptl4*, *Map3k13*, *Slc31a2*, *Abcb1b*, *Slc6a9*, *Slc5a1* and *Erbb3*) were related to glucose metabolism and cellular energy metabolism, with *Igfbp1* and *Angptl4* showing as the top ranking two signals (Fig. 3F). To further identify transcriptome differences related to glucose and energy metabolism, the mRNA expression levels of these eight genes were further determined by qPCR (Figs. 3G and S3A–F). Results accurately showed that DN enhanced *Igfbp1* ($P < 0.05$) and *Angptl4* ($P < 0.05$) compared to Control group. Compared with DN group, DN + GLP significantly decreased the expression level of *Igfbp1* and *Angptl4* ($P < 0.05$). Altogether, these findings indicated that GLP

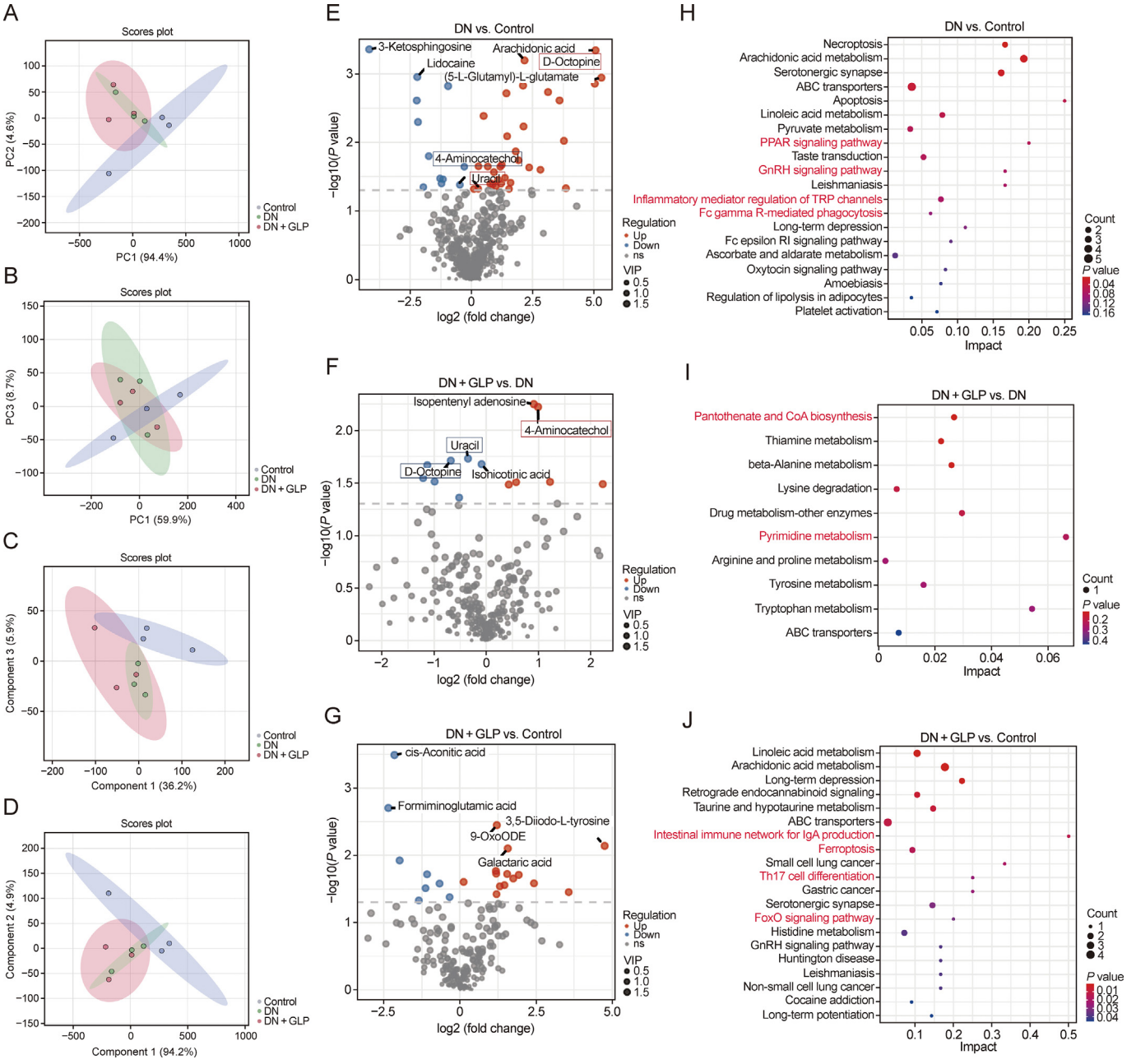

Fig. 5. Metabolomic analysis under the positive and negative ion mode ($n = 3$). (A–D) Principal component analysis (PCA) and orthogonal partial least squares discriminant analysis (OPLS-DA) score plots depicting the comparison of metabolomic profiles among Control, diabetic nephropathy (DN), and sporoderm-broken spores of *Ganoderma lucidum* (GLP)-treated high-fat diet (HFD)-fed (DN + GLP) group. PCA score plot under positive ion mode (A), PCA score plot under negative ion mode (B), OPLS-DA score plot under positive ion mode (C), OPLS-DA score plot under negative ion mode (D). (E–G) Volcano plot of differentially accumulated metabolites in three groups including DN vs. Control (E), DN + GLP vs. DN (F), DN + GLP vs. Control (G). (H–J) Kyoto Encyclopedia of Genes and Genomes (KEGG) pathways enrichment analysis of differentially accumulated metabolites in three groups including DN vs. Control (H), DN + GLP vs. DN (I), and DN + GLP vs. Control (J). Red dots, upregulated; blue dots, downregulated.FC: fold change; VIP: variable importance; ABC: ATP-binding cassette; PPAR: peroxisome proliferators-activated receptor; GnRH: gonadotropin-releasing hormone; TRP: transient receptor potential; RI: refractive index; CoA: coenzyme A; Th17: *IL-17*-producing T helper; FoxO: orkhead box transcription factors class O.

intervention had much effect on modulating kidney transcription in a variety of glucose and energy metabolism molecular processes.

The abundance of possible signalling pathways induced by dietary components and GLP intervention was estimated by GO enrichment analysis. DN vs. Control yielded the most abundant DEGs, response to vitamin, regulation of cell growth, humoral immune response mediated by circulating immunoglobulin and immunoglobulin mediated immune response were the main biological processes (Fig. 4A and Table S5). Circadian regulation of gene expression, response to glucose, and phosphatidylinositol metabolic process were mostly enriched in DN + GLP vs. DN (Fig. 4B and Table S6). Response to nutrient, metabolic process, response to hypoxia, and sulfur compound metabolic process were enriched in DN + GLP when compared to Control (Fig. 4C and Table S7). KEGG analysis was then carried out for the DEGs that were acquired from each of the three subgroups, which yielded the results of enriched pathways directly associated with advanced glycation endproduct-receptor for advanced glycation endproducts (AGE-RAGE) signalling pathway in diabetic complications and phosphoinositide 3-kinase (PI3K) - protein kinase B (AKT) signalling pathway in DN vs. Control (Fig. 4D and Table S8), phospholipase D signalling pathway, parathyroid hormone synthesis, secretion and action, and glycine, serine and threonine metabolism in DN + GLP vs. DN (Fig. 4E and Table S9), mammalian target of rapamycin (mTOR) signalling pathway, and inflammatory mediator regulation of the transient receptor potential (TRP) channels in DN + GLP vs. Control (Fig. 4F and Table S10). Interestingly, our analysis revealed that metabolic process pathway was primarily enriched in all group comparisons according to KEGG enrichment analysis.

3.3. Effects of GLP supplementation on nephritic metabolic profiles

Ultra performance liquid chromatography-tandem mass spectrometry (UPLC-MS/MS) was performed to examine metabolic differences between Control vs. DN, DN vs. DN + GLP, and Control vs. DN + GLP comparisons. There was a total of 495 annotated metabolites identified. Significant differences among all groups were found by PCA analysis in both positive and negative models (Figs. 5A–D). 44 metabolites in DN group had VIP scores > 1.5 and $P < 0.05$ in comparison with Control (Fig. 5E and Table S11), i.e., 3-

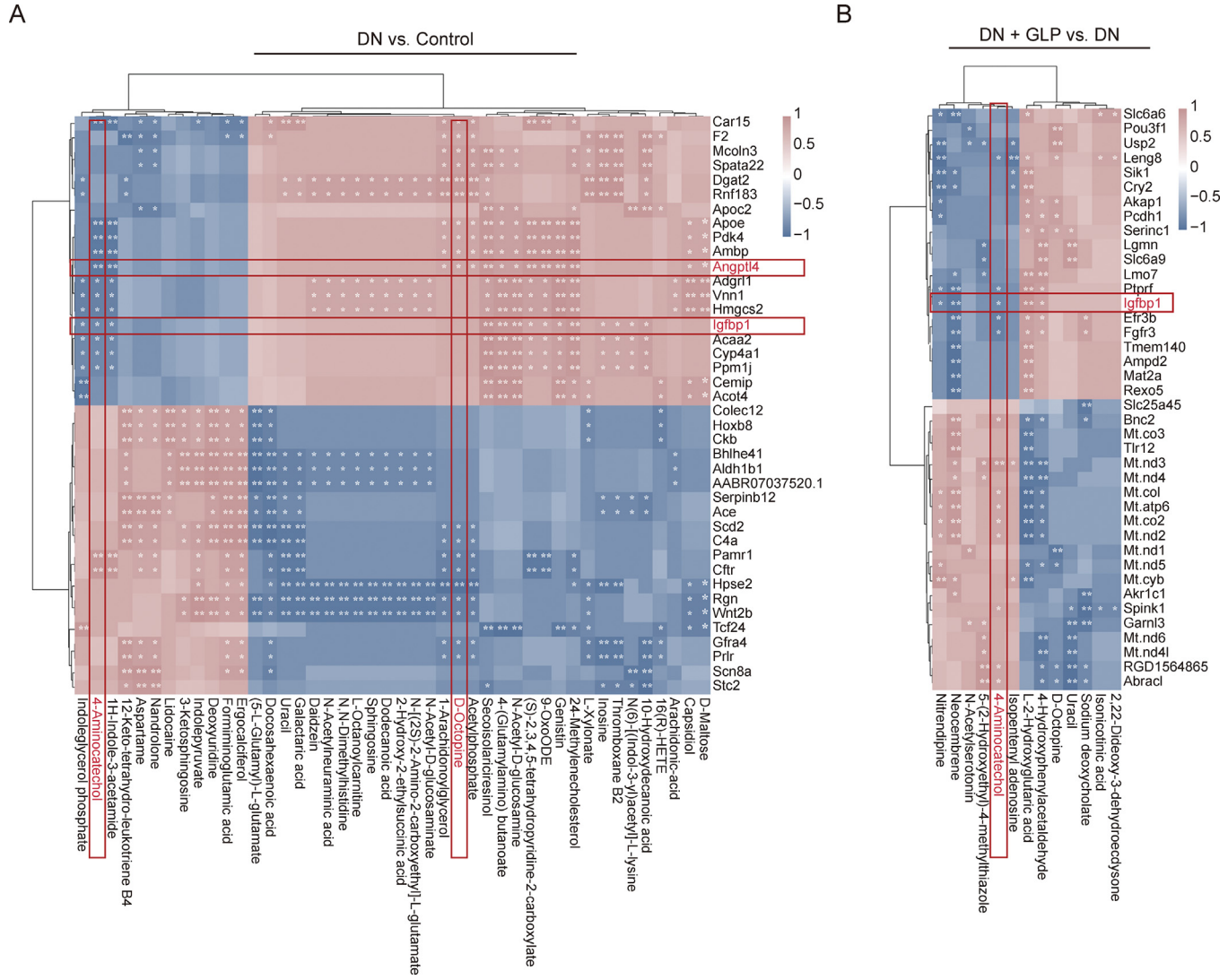

Fig. 6. Correlation analysis amongst differentially expressed genes (DEGs) and differentially accumulated metabolites. (A, B) Spearman's correlation of metabolome and transcriptome analysis in diabetic nephropathy (DN) vs. Control (A), and sporoderm-broken spores of *Ganoderma lucidum* (GLP)-treated high-fat diet (HFD)-fed (DN + GLP) vs. DN (B). $^{*}P < 0.05$, $^{**}P < 0.01$ and $^{***}P < 0.001$.

ketosphingosine (VIP = 1.97), D-octopine (VIP = 1.96), and (5-L-glutamyl)-L-glutamate (VIP = 1.95). 13 metabolites had VIP scores > 1.5 and $P < 0.05$ in DN + GLP relative to DN group (Fig. 5F and Table S12), i.e., isopentenyl adenosine (VIP = 2.23), 4-Aminocatechol (VIP = 2.12), and D-octopine (VIP = 2.01). 22 metabolites had VIP scores > 1.5 and $P < 0.05$ in DN + GLP when comparing to Control (Fig. 5G and Table S13), i.e., cis-aconitic acid (VIP = 1.80), formiminoglutamic acid (VIP = 1.76), and 9-OxoODE (VIP = 1.74). OPLS-DA analysis indicated that potential metabolites including 4-Aminocatechol were significantly decreased in DN model compared to Control ($P < 0.05$), and increased abundance of D-Octopine and Uracil was observed in DN relative to Control groups. Nevertheless, GLP treatment reversed this trend (Figs. 5E and F). Differential metabolites between DN and Control were mostly enriched in Fc epsilon refractive index (RI) signalling pathway, inflammatory mediator regulation of TRP channels, peroxisome proliferators-activated receptors (PPARs) and gonadotropin-releasing hormone (GnRH) signalling pathway according to KEGG enrichment analysis (Fig. 5H). In comparison of DN + GLP and DN, differential metabolic features mainly enriched in pantothenate and coenzyme A (CoA) biosynthesis and pyrimidine metabolism (Fig. 5I). For the comparison of DN + GLP and Control, pathways of *IL-17*-producing T helper (Th17) cell differentiation, Intestinal immune network for IgA production, and forkhead box transcription factors class O (FoxO) signalling pathway were similarly enriched (Fig. 5J). Additionally, the network analysis of key differential metabolites and KEGG general metabolic pathway was visualized in Figs. S4A and B.

3.4. Integrated analysis of metabolome and transcriptome in energy metabolism

To further investigate the changes in metabolic pathway response to GLP intervention, a comprehensive correlation analysis was carried out by integrating differential metabolites and DEGs. Here, the correlation between differential metabolites and top 40 DEGs (20 downregulated and 20 upregulated DEGs, respectively) was examined using Spearman's correlation coefficient. As shown in Figs. 6A and B, and S5, *Angptl4* was negatively correlated with 4-Aminocatechol and positively correlated with D-Octopine, and *Igfbp1* was negatively correlated with D-Octopine in DN relative to Control ($P < 0.05$) (Fig. 6A). *Igfbp1* showed a significantly negative correlation with 4-Aminocatechol in DN + GLP compared to DN (Fig. 6B). Collectively, these correlation findings indicated that GLP could alleviate the influence of high-fat dietary factors by regulating key genes expression level and metabolic biomarkers in rats.

3.5. Validation analysis in human DN

Considering that transcriptomic regulations have been identified as independent biomarkers of human disease, validation analysis was performed for the transcriptomic comparison between DN patients and healthy controls utilizing human transcriptome data (GSE104954 dataset). Fig. S6A presented the DEGs between DN patients and healthy controls. It was apparently indicated that immune cytokines (i.e., *CXCL6* and *CX3CR1*) upregulated in DN patients. Figs. S6B and C showed the expression level of *Igfbp1* and *Angptl4*, which were key signatures identified from DN rat model, and *Igfbp1* was significantly overexpressed in DN patients ($P < 0.05$). As shown in Figs. S6D and E, 405 GO enrichment pathways and 15 KEGG pathways transcriptional level changed. Consistent with our above findings from rats' DN model, GO pathways were related to immune-associated pathways including positive regulation of cytokine production and humoral immune response, and cellular metabolism pathways (Fig. S6D). Amongst the KEGG pathways, autoimmune diseases (i.e., rheumatoid arthritis and asthma) and AGE-RACE signalling pathways in diabetic complications were verified in the present study, which consistently indicated the immunoregulation in DN (Fig. S6E). Immune cytokines (*CX3CR1, CXCL6* and *LIT*) were further validated among DN and DN + GLP rats, results suggested that DN rats showed higher immune infiltration than Control group, and GLP treatment could lower these inflammatory factors levels consistently (Figs. S6F–H).

3.6. The nephritic pharmacological function of GLP by integrating NP

Eighty-eight active targets in GLP were obtained from the GeneCards, OMIM, and PharmGKB databases after removing duplicates (Fig. 7A). According to DrugBank, DisGeNET, TTD and GeneCards databases, 1,720 possible targets of DN were retrieved (Fig. 7B). Thirty-three common targets were showed in a Venn diagram and used for further investigation (Fig. 7C). Afterwards, protein interaction networks of the constituents and putative targets of DN disease were constructed using STRING database, acquiring 33 nodes and 138 edges in the STRING results (Fig. 7D). The findings suggested that immune-related proteins (CXCL8, FBJ murine osteosarcoma viral oncogene homolog (FOS), toll-like receptor 4 (TLR4), IL-10, IL-4) could be possible targets for DN. Ten key targets above were confirmed by topological network analysis of crucial nodes based on 11 algorithms (Figs. 7E and S7). The String and ChiPlot platforms were used to perform KEGG analysis based on the common targets of active GLP-DN. Top 20 significantly enriched pathways were identified in our study, including PD-L1 expression and PD-1 checkpoint pathway in cancer, IL-17 signalling pathway, Toll-like receptor signalling pathway, Cytokine-cytokine receptor signalling pathway, and T cell receptor signalling pathway (Figs. 7F and G). These findings stimulate the potential mechanisms for GLP in treating DN by immunoregulation, supporting the above findings from transcriptome and metabolome analysis.

4. Discussion

Studies have shown that GLP had a wide array of pharmacological properties, such as antioxidant, immunomodulatory effects [29,30], anticancer [31], regulating blood glucose levels, hepatoprotective effects, neuroprotective properties, etc. [30,32,33]. Accumulating evidence supports the link between disturbances of metabolism levels and DN [34], which provides potential new therapeutic avenues for patients with DN. These diverse pharmacological properties underscore the potential of GLP as a multifaceted natural therapeutic agent for DN. In this experimental-based research, we firstly investigated the role of GLP treatment on kidney function of HFD-induced DN by transcriptome, metabolome, and NP analyses. Then examined the correlation between differential metabolites and the key features of gene expression, aiming to illustrate potential beneficial effects of GLP. In our study, we revealed that the GLP treatment improved kidney damage and inflammation levels in DN rats (Figs. 1, 2, S1, and S2).

The kidney is essential for energy metabolism and glucose circulation [35,36]. Nephritic transcriptome was conducted to understand the amelioration of GLP on renal-associated metabolic processes (Figs. 3, 4, and S3). Notably, GLP profoundly altered the glucose metabolism-related and cellular energy metabolism-related genes in the kidney (such as *Igfbp1* and *Angptl4*) upregulated in DN group compared to Control group, and downregulated after GLP treatment. Dysregulation of insulin-like growth factor binding protein 1 (IGFBP-1) as well as insulin-like growth factors

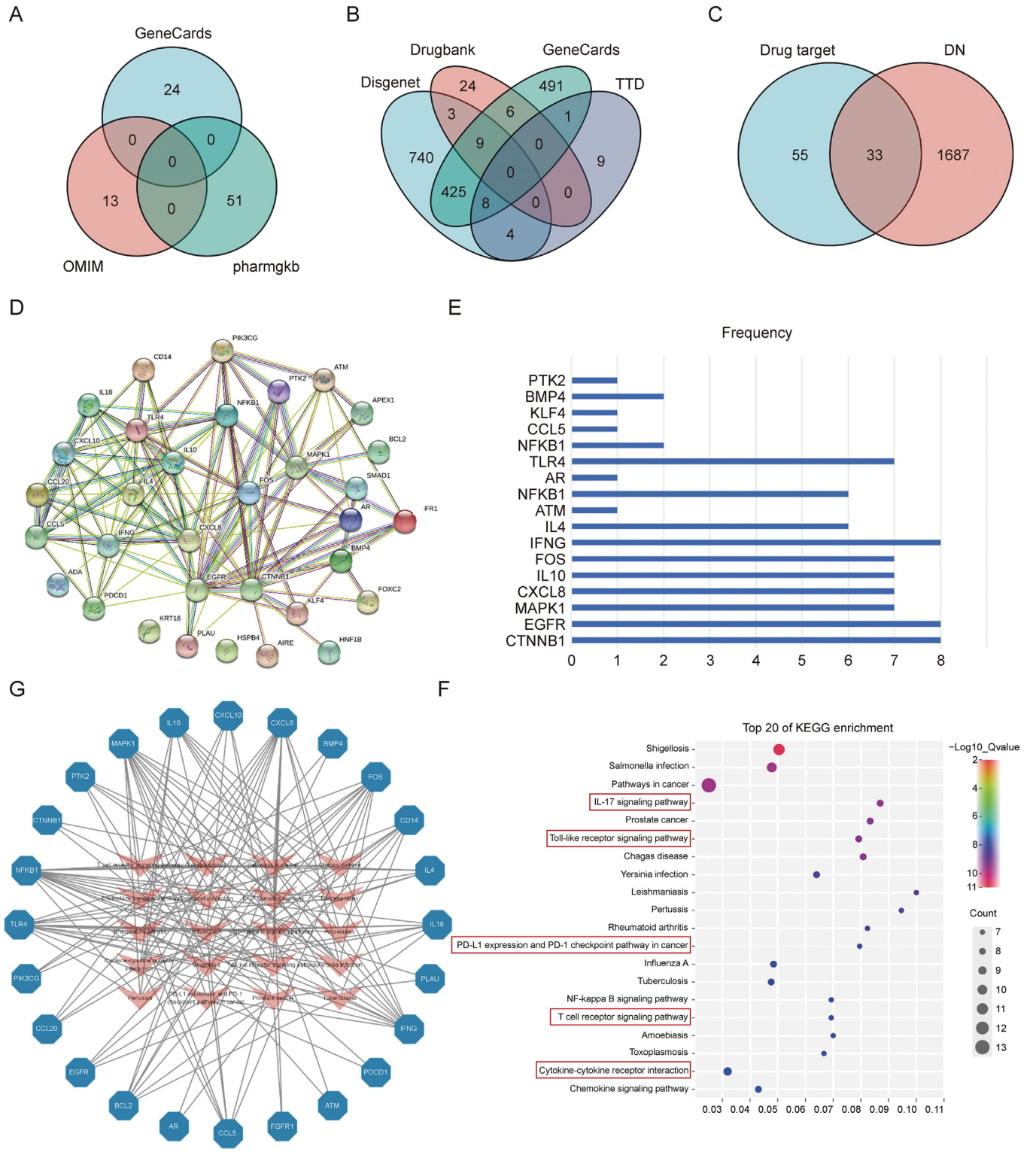

Fig. 7. Network pharmacology (NP) of intersecting targets of sporoderm-broken spores of *Ganoderma lucidum* (GLP) towards diabetic nephropathy (DN). (A) Screening of GLP targets. (B) Screening of DN-related targets. (C) Venn diagram showed the common targets of DN and GLP. (D) Protein–protein interaction (PPI) network analysis of drug-disease intersection targets. (E) Frequency of the top 10 most frequent target genes based on 11 algorithms. (F) Top 20 Kyoto Encyclopedia of Genes and Genomes (KEGG) pathway enrichment analysis of key targets ($P < 0.05$). Key targets and pathways are marked with red rectangles. (G) Visualization of KEGG pathways and selected key targets through Cytoscape. DN + GLP: GLP-treated high-fat diet (HFD)-fed group; TTD, therapeutic target database; IL: interleukin; CXCL: C-X-C motif chemokine ligand; TLR4: toll-like receptor 4; CCL: C-C motif chemokine ligand; FOS: FBJ murine osteosarcoma viral oncogene homolog; MAPK: mitogen activated protein kinase.

(IGFs) in serum induces metabolic disorders (e.g., type 2 diabetes) and cardiovascular disease [37]. Another clinical observation has demonstrated that higher circulating IGFBP-1 levels are linked to type 1 diabetes (T1D) and DN [38]. Meanwhile, levels of circulating *Angptl4* showed a significant increase in patients with DN, interestingly, the elevation in *Angptl4* correlated significantly with

clinical markers of DN including serum creatinine, epidermal growth factor receptor (eGFR), as well as IGFBP-1 [39]. These results suggested that the *Igfbp1* and *Angptl4* levels were probably attributed to the regulation of development of DN. Combined with enriched GO terms and KEGG pathway, the study revealed that GLP may alleviate DN through the regulation of genes related to glucose metabolism and energy metabolism.

Evidence of DN-induced energy expenditure and glucose metabolism contributes to chronic inflammatory status. Complementary data extracted from patients with DN and healthy controls, findings about immune regulating genes and higher *Igfbp1* expression level in DN patients were identified, consistently indicating the immunoregulation in DN (Fig. S6). As expected, the therapeutic targets of GLP identified by metabolome and NP method were immune-related proteins, such as inflammatory cytokines (i.e., *CXCL8*, *FOS*, *TLR4*). Nephritic metabolome further indicated the distinct differences in DN and GLP treatment (Figs. 5 and S4). The abundance of potential biomarkers of D-Octopine and Uracil was shown to be significantly increased by DN. Additionally, significant decrease of 4-Aminocatechol was identified with DN model. Further integration transcriptome and metabolome analysis hinted that 4-Aminocatechol was negatively correlated with genes enriched in the energy metabolism pathway and inflammatory response, suggesting that 4-Aminocatechol might be vital in regulating inflammation and metabolic changes (Figs. 5, 6, S4 and S5). Collectively, these findings could provide a better understanding of GLP alleviate kidney damage by suppressing the expression of *Igfbp1* and *Angptl4* through glucose related and energy metabolism pathways, and enhancing immunoregulation (Fig. 8).

Recent studies have suggested several potential mechanisms that *G. lucidum* may improve DN-related kidney injury, including PI3K/AKT/mTOR signalling pathway [16], autophagy activation [16], anti-apoptotic effects [40], and inflammatory pathways [41], which were verified by our multi-omics data (Figs. 3–7). Taken the findings together, it suggested that GLP treatment alleviates inflammation and renal injury by reducing inflammatory cytokines (such as *CXCL6* and *CX3CR1*) and suppressing *Igfbp1* and *Angptl4* expression in renal tissues. The potential mechanisms through which GLP exerts its effects on glucose metabolism may involve enhancing insulin sensitivity by upregulating the expression and translocation of glucose transporter 4 (GLUT4) [42], suppressing hepatic gluconeogenesis-related enzymes such as phosphoenolpyruvate carboxykinase (PEPCK) and glucose-6-phosphatase (G6Pase) [43], activating AMP-activated protein kinase (AMPK) to promote glucose uptake and fatty acid oxidation [44], and enhancing the incretin effect [45]. Moreover, the potential mechanisms by which GLP exerts its effects on inflammation may be involved in suppressing the nuclear factor-kappa B (NF-κB) signalling pathway, activating mitogen activated protein kinase (MAPK) pathways, particularly p38 and extracellular regulated kinase 1/2 (ERK1/2), enhancing the activity of antioxidant enzymes such as superoxide dismutase (SOD) and catalase, and inhibiting the Nod-like receptor family pyrin domain containing 3 (NLRP3) inflammasome [46–48]. To date, the precise molecular mechanisms by which GLP ameliorates DN still require further validation and human clinical studies.

While our study focused on the effects of GLP in its native form, recent advancements in nanomedicine offer exciting possibilities for enhancing its therapeutic potential. For example, Zhang et al. [49] created GLP-coated gold nanoparticles with enhanced antioxidant and immunomodulatory activities. Similarly, another study developed GLP-loaded chitosan nanoparticles with improved stability and enhanced immunomodulatory effects [50]. These nanoformulation approaches could potentially be applied to our findings to further improve GLP's efficacy in treating DN. Future studies could explore the use of such nanocarriers to enhance GLP delivery to the kidneys, potentially amplifying its beneficial effects on glucose metabolism, inflammation, and renal function as identified in our multi-omics analysis. However, limitations and unresolved issues should be acknowledged that i) these findings are lacking

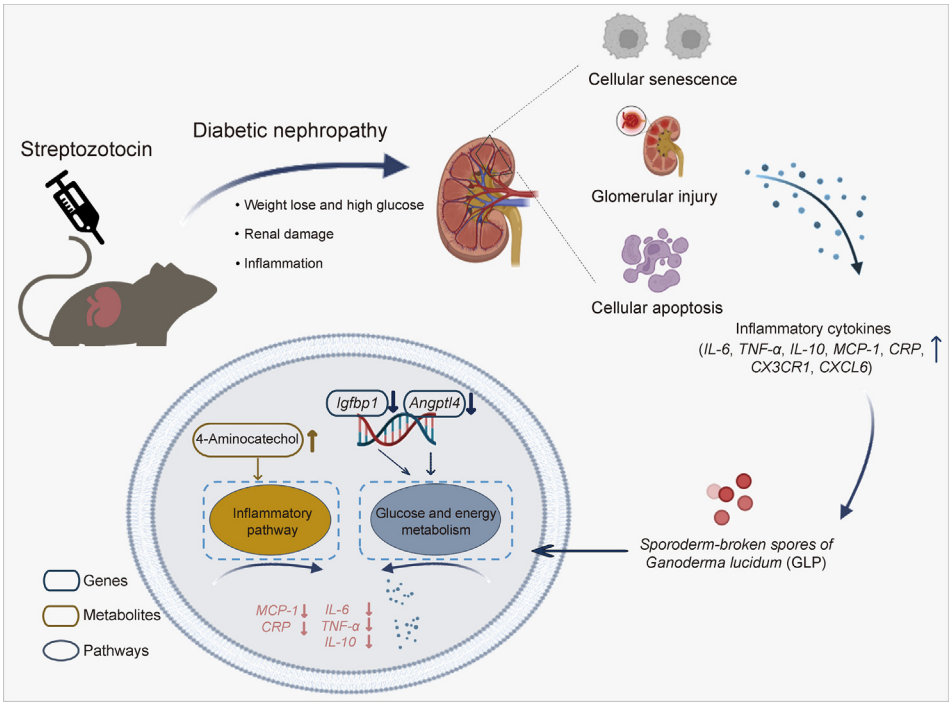

Fig. 8. Proposed mechanism of sporoderm-broken spores of *Ganoderma lucidum* (GLP) treatment on ameliorating diabetic nephropathy (DN) rats. IL: interleukin; TNF-α: tumor necrosis factor-alpha; MCP-1: monocyte chemoattractant protein-1; CRP: C-reactive protein ; CX3CR1: C-X3-C motif chemokine receptor 1; CXCL: C-X-C motif chemokine ligand.

clinical manifestations as seen in DN patients; ii) though we have revealed potential protective and anti-immunity role of GLP in DN rats, further exploration is required to compare the specific therapeutic effects of GLP with other herbal medicine known for the therapy of DN; and iii) the molecular mechanisms of downstream regulatory key molecules on metabolome disturbance resulting from an DN model are unclear. More thorough profiles of GLP utilization in vivo and targeted metabolomic analysis are needed to ascertain our findings in additional studies.

5. Conclusion

In sum, this is the first study to demonstrate that low dose of GLP improved renal damage and inflammation levels in DN rat models. Our analysis of transcriptomic data from DN patients and healthy controls revealed elevated expression of key genes, including IGF-related genes and inflammatory cytokines in DN patients. Importantly, these findings align with and validate our observations in the DN rat model. Specifically, these results potentially showed that GLP treatment ameliorated DN by suppressing the expression of *Igfbp1* and *Angptl4* and enhancing metabolic biomarkers of 4-Aminocatechol through glucose related and energy metabolism pathways, and enhancing immunoregulation. This comprehensive integration analysis using transcriptomics, metabolomics, and NP represents an advanced analytical approach in pharmaceutical research, which also highlights the possibility of the future application of GLP as a protective and anti-immunity therapeutic herb in DN patients.

Ethical approval

The Ethics Committee of Zhejiang University has given the approval for this research (No. 22016), and the “Chinese Animal Ethics Standards and Guidelines” were strictly followed in animal experiments of this project.

CRediT authorship contribution statement

Lidan Hu: Conceptualization, Funding acquisition, Methodology, Project administration, Supervision. **Lili Yu:** Data curation, Formal analysis, Methodology, Visualization, Writing – original draft, Writing – review & editing. **Zhongkai Cao:** Data curation, Investigation. **Yue Wang:** Investigation. **Caifeng Zhu:** Investigation. **Yayu Li:** Writing – review & editing. **Jiazhen Yin:** Writing – review & editing. **Zhichao Ma:** Writing – review & editing. **Xuelin He:** Writing – review & editing. **Ying Zhang:** Writing – review & editing. **Wunan Huang:** Writing – review & editing. **Yuelin Guan:** Writing – review & editing. **Yue Chen:** Supervision, Writing – review & editing. **Xue Li:** Supervision, Writing – review & editing. **Xiangjun Chen:** Project administration, Resources, Supervision.

Declaration of competing interest

The authors declare that there are no conflicts of interest.

Acknowledgments

This work was supported by the National Natural Science Foundation of China (Grant Nos.: 32271311 and 82200784 to Lidan Hu). The authors express great appreciation to all former and current members of Hu's Lab and Chen's Lab, for the insightful conversation and outstanding contributions of this research. We are also grateful to Yingping Xiao for professional expert in the experimental processes.

Appendix A. Supplementary data

Supplementary data to this article can be found online at https://doi.org/10.1016/j.jpha.2024.101105.

References

[1] L. Chen, D.J. Magliano, P.Z. Zimmet, The worldwide epidemiology of type 2 diabetes mellitus: Present and future perspectives, Nat.Rev. Endocrinol. 8 (2011) 228–236.
[2] F. Giacco, M. Brownlee, Oxidative stress and diabetic complications, Circ. Res. 107 (2010) 1058–1070.
[3] B. Giri, S. Dey, T. Das, et al., Chronic hyperglycemia mediated physiological alteration and metabolic distortion leads to organ dysfunction, infection, cancer progression and other pathophysiological consequences: An update on glucose toxicity, Biomed. Pharmacother. 107 (2018) 306–328.
[4] S. Huang, M. Tan, F. Guo, , et al.C.Y. Nepeta angustifolia, Wu improves renal injury in HFD/STZ-induced diabetic nephropathy and inhibits oxidative stress-induced apoptosis of mesangial cells, J. Ethnopharmacol. 255 (2020), 112771.
[5] S. Zheng, D.W. Powell, F. Zheng, et al., Diabetic nephropathy: Proteinuria, inflammation, and fibrosis, J. Diabetes Res. 2016 (2016), 5241549.
[6] Z. Li, Y. Shi, X. Zhang, et al., Screening immunoactive compounds of *Ganoderma lucidum* spores by mass spectrometry molecular networking combined with *in vivo* zebrafish assays, Front. Pharmacol. 11 (2020), 287.
[7] J. Su, L. Su, D. Li, et al., Antitumor activity of extract from the sporoderm-breaking spore of *Ganoderma lucidum*: Restoration on exhausted cytotoxic T cell with gut microbiota remodeling, Front. Immunol. 9 (2018), 1765.
[8] E. Ekiz, E. Oz, A.M. Abd El-Aty, et al., Exploring the potential medicinal benefits of *Ganoderma lucidum*: From metabolic disorders to coronavirus infections, Foods 12 (2023), 1512.
[9] A.M. F, *Ganoderma lucidum*: Persuasive biologically active constituents and their health endorsement, Biomed. Pharmacother. 107 (2018) 507–519.
[10] S. Cheng, D. Sliva, *Ganoderma lucidum* for cancer treatment: We are close but still not there, Integr. Cancer Ther. 14 (2015) 249–257.
[11] R. Cui, F. Zhu, Ultrasound modified polysaccharides: A review of structure, physicochemical properties, biological activities and food applications, Trends Food Sci. Technol. 107 (2021) 491–508.
[12] C. Gong, M.C. Lee, M. Godec, et al., Ultrasonic encapsulation of cinnamon flavor to impart heat stability for baking applications, Food Hydrocoll. 99 (2020), 105316.
[13] Y. Wang, X. Fan, X. Wu, *Ganoderma lucidum* polysaccharide (GLP) enhances antitumor immune response by regulating differentiation and inhibition of MDSCs *via* a CARD9-NF-κB-IDO pathway, Biosci. Rep. 40 (2020), BSR20201170.
[14] H. Zhao, Q. Zhang, L. Zhao, et al., Spore Powder of *Ganoderma lucidum* improves cancer-related fatigue in breast cancer patients undergoing endocrine therapy: A pilot clinical trial, Evid. Based Complement. Alternat. Med. 2012 (2012), 809614.
[15] H.M. Akshay Kumar, M. Sarkar, K. Darshan, et al., The *Ganoderma*: Biodiversity and Significance. Fungal Biology, Springer Nature, Singapore, 2022, pp. 255–291.
[16] Y. Hu, S. Wang, F. Wu, et al., Effects and mechanism of *Ganoderma lucidum* polysaccharides in the treatment of diabetic nephropathy in streptozotocin-induced diabetic rats, BioMed Res. Int. 2022 (2022), 4314415.
[17] C. Guo, D. Guo, L. Fang, et al., *Ganoderma lucidum* polysaccharide modulates gut microbiota and immune cell function to inhibit inflammation and tumorigenesis in colon, Carbohydr. Polym. 267 (2021), 118231.
[18] X. Geng, D. Zhong, L. Su, et al., Preventive and therapeutic effect of *Ganoderma lucidum* on kidney injuries and diseases, Adv. Pharmacol. 87 (2020) 257–276.
[19] M.F. Ahmad, F.A. Ahmad, N. Hasan, et al., *Ganoderma lucidum*: Multifaceted mechanisms to combat diabetes through polysaccharides and triterpenoids: A comprehensive review, Int. J. Biol. Macromol. 268 (2024), 131644.
[20] H.M. Colhoun, M.L. Marcovecchio, Biomarkers of diabetic kidney disease, Diabetologia 61 (2018) 996–1011.
[21] H. Wu, R. Gonzalez Villalobos, X. Yao, et al., Mapping the single-cell transcriptomic response of murine diabetic kidney disease to therapies, Cell Metab. 34 (2022) 1064–1078.e6.
[22] F. Persson, P. Rossing, Diagnosis of diabetic kidney disease: State of the art and future perspective, Kidney Int. Suppl. 8 (2018) 2–7.
[23] Y. Zhao, Y. Qin, X. Hu, et al., Sporoderm-removed *Ganoderma lucidum* spores ameliorated early depression-like behavior in a rat model of sporadic Alzheimer's disease, Front. Pharmacol. 15 (2024), 1406127.
[24] H. Zhao, S. Cui, Y. Qin, et al., Prophylactic effects of sporoderm-removed *Ganoderma lucidum* spores in a rat model of streptozotocin-induced sporadic Alzheimer's disease, J. Ethnopharmacol. 269 (2021), 113725.
[25] L. Xia, R. Sun, L. Zhang, et al., A 26-week repeated dose toxicity evaluation of sporoderm-removed *Ganoderma lucidum* spores in rats, Food Chem. Toxicol. 182 (2023), 114175.
[26] K. Su, B. Yi, B. Yao, et al., Liraglutide attenuates renal tubular ectopic lipid deposition in rats with diabetic nephropathy by inhibiting lipid synthesis and promoting lipolysis, Pharmacol. Res. 156 (2020), 104778.
[27] L. Zhu, J. Han, R. Yuan, et al., Berberine ameliorates diabetic nephropathy by inhibiting TLR4/NF-κB pathway, Biol. Res. 51 (2018), 9.

[28] Y. Xiong, L. Zhou, The signaling of cellular senescence in diabetic nephropathy, Oxid. Med. Cell. Longev. 2019 (2019), 7495629.
[29] S. Huang, Z. Ning, Extraction of polysaccharide from *Ganoderma lucidum* and its immune enhancement activity, Int. J. Biol. Macromol. 47 (2010) 336–341.
[30] W. Zhang, Z. Lei, J. Meng, et al., Water extract of sporoderm-broken spores of *Ganoderma lucidum* induces osteosarcoma apoptosis and restricts autophagic flux, Onco. Targets Ther. 12 (2019) 11651–11665.
[31] X. Jin, J. Ruiz Beguerie, D.M. Sze, et al., *Ganoderma lucidum* (Reishi mushroom) for cancer treatment, Cochrane Database Syst. Rev. 4 (2016), CD007731.
[32] A. Barbieri, V. Quagliariello, V. del Vecchio, et al., Anticancer and anti-inflammatory properties of *Ganoderma lucidum* extract effects on melanoma and triple-negative breast cancer treatment, Nutrients 9 (2017), 210.
[33] H.J. Janse van Rensburg, T. Azad, M. Ling, et al., The hippo pathway component TAZ promotes immune evasion in human cancer through PD-L1, Cancer Res. 78 (2018) 1457–1470.
[34] L. Chen, X. Chen, X. Huang, et al., Regulation of glucose and lipid metabolism in health and disease, Sci. China Life Sci. 62 (2019) 1420–1458.
[35] M. Alsahli, J.E. Gerich, Renal glucose metabolism in normal physiological conditions and in diabetes, Diabetes Res. Clin. Pract. 133 (2017) 1–9.
[36] R. Fernandes, The controversial role of glucose in the diabetic kidney, Porto Biomed. J. 6 (2021), e113.
[37] V.A. Ezzat, E.R. Duncan, S.B. Wheatcroft, et al., The role of IGF-I and its binding proteins in the development of type 2 diabetes and cardiovascular disease, Diabetes Obes. Metab. 10 (2008) 198–211.
[38] T. Gu, H. Falhammar, H.F. Gu, et al., Epigenetic analyses of the insulin-like growth factor binding protein 1 gene in type 1 diabetes and diabetic nephropathy, Clin. Epigenetics 6 (2014), 10.
[39] E. Al Shawaf, M. Abu-Farha, S. Devarajan, et al., ANGPTL4: A predictive marker for diabetic nephropathy, J. Diabetes Res. 2019 (2019), 4943191.
[40] H.M. Hassan, Y.F. Mahran, A.M.H. Ghanim, *Ganoderma lucidum* ameliorates the diabetic nephropathy *via* down-regulatory effect on TGFβ-1 and TLR-4/NFκB signalling pathways, J. Pharm. Pharmacol. 73 (2021) 1250–1261.
[41] J.F. Navarro-González, C. Mora-Fernández, The role of inflammatory cytokines in diabetic nephropathy, J. Am. Soc. Nephrol. 19 (2008) 433–442.
[42] C. Xiao, Q. Wu, W. Cai, et al., Hypoglycemic effects of *Ganoderma lucidum* polysaccharides in type 2 diabetic mice, Arch. Pharm. Res. 35 (2012) 1793–1801.
[43] S.W. Seto, T.Y. Lam, H.L. Tam, et al., Novel hypoglycemic effects of *Ganoderma lucidum* water-extract in obese/diabetic (+db/+db) mice, Phytomedicine 16 (2009) 426–436.
[44] H. Xue, J. Qiao, G. Meng, et al., Effect of *Ganoderma lucidum* polysaccharides on hemodynamic and antioxidation in T2DM rats, Zhongguo Zhong Yao Za Zhi 35 (2010) 339–343.
[45] C.J. Chang, C. Lin, C.C. Lu, et al., *Ganoderma lucidum* reduces obesity in mice by modulating the composition of the gut microbiota, Nat. Commun. 6 (2015), 7489.
[46] S. Dudhgaonkar, A. Thyagarajan, D. Sliva, Suppression of the inflammatory response by triterpenes isolated from the mushroom *Ganoderma lucidum*, Int. Immunopharmacol. 9 (2009) 1272–1280.
[47] C. Cheng, A.Y. Leung, C.F. Chen, The effects of two different *Ganoderma* species (Lingzhi) on gene expression in human monocytic THP-1 cells, Nutr. Cancer 62 (2010) 648–658.
[48] J. Xie, D. Lin, J. Li, et al., Effects of *Ganoderma lucidum* polysaccharide peptide ameliorating cyclophosphamide-induced immune dysfunctions based on metabolomics analysis, Front. Nutr. 10 (2023), 1179749.
[49] S. Zhang, G. Pang, C. Chen, et al., Effective cancer immunotherapy by *Ganoderma lucidum* polysaccharide-gold nanocomposites through dendritic cell activation and memory T cell response, Carbohydr. Polym. 205 (2019) 192–202.
[50] G. Pang, S. Zhang, X. Zhou, et al., Immunoactive polysaccharide functionalized gold nanocomposites promote dendritic cell stimulation and antitumor effects, Nanomedicine (Lond) 14 (2019) 1291–1306.